East European Journal of Physics. **4.** 442-448 (2025)
DOI:10.26565/2312-4334-2025-4-44 ISSN 2312-4334

BANDGAP-ENGINEERED pSi/n-Cd_xS_{1-x} HETEROJUNCTIONS: EFFECT OF COMPOSITION ON OPTOELECTRONIC BEHAVIOR

Ibrokhim B. Sapaev[1,2,4,5]*, Jamoliddin I. Razzokov[6,7], Jo'shqin Sh. Abdullayev[1], Dildora A. Qalandarova[3], Madinabonu Sh. Ibragimova[3]

[1]*National Research University TIIAME, Department «Physics and Chemistry», Kori Niyoziy 39, Tashkent 100000, Uzbekistan*
[2]*Tashkent University for Applied Sciences, 28 Universitetskaya Street, Tashkent 100095, Uzbekistan*
[3]*Urgench State University, Hamid Olimjon Street, 14, Urgench, 220100 Uzbekistan*
[4]*School of Engineering, Central Asian University, Tashkent 111221, Uzbekistan*
[5]*Azerbaijan State Oil and Industry University (ASOIU), Faculty of Chemical Technology, 20 Azadlig Avenue, Baku AZ1010, Azerbaijan*
[6]*Institute of Fundamental and Applied Research, National Research University TIIAME, Kori Niyoziy 39, Tashkent 100000, Uzbekistan*
[7]*Department of Biotechnology, Tashkent State Technical University, Universitet 2, 100095, Tashkent, Uzbekistan*
**Corresponding Author e-mail: j.sh.abdullayev6@gmail.com*
Received June 28, 2025; revised October 11, 2025; in final form October 20, 2025; accepted October 21, 2025

This study provides a comprehensive analysis of the electrophysical properties of the pSi/n-Cd_xS_{1-x} heterojunction, where the cadmium composition x varies continuously from 0 to 1. The investigation integrates theoretical modeling, numerical simulations, and experimental validation employing typical doping concentrations of $p = 2\times10^{17}$ cm^{-3} for p-type porous silicon and $n = 1\times10^{18}$ cm^{-3} for n-type Cd_xS_{1-x}. Particular attention is devoted to the temperature-dependent evolution of key material parameters, including the bandgap energy Eg(T), intrinsic carrier concentration $n_i(T)$, and the Debye temperature $\Theta(x)$. As the cadmium fraction increases, the bandgap narrowing in Cd_xS_{1-x} becomes evident, while porous silicon maintains a relatively wide and thermally stable Eg(T), resulting in a substantial band offset (ΔEg) that enhances charge carrier separation across the interface. Furthermore, the reduction of $\Theta(x)$ with increasing cadmium concentration modulates phonon scattering and recombination dynamics, thereby influencing charge transport characteristics. The analysis of current transport mechanisms indicates that the junction behavior is predominantly controlled by temperature- and composition-dependent band alignment and carrier recombination processes. The obtained results validate the proposed physical model and demonstrate the promising potential of pSi/n-Cd_xS_{1-x} heterostructures for high-temperature and acoustically tunable optoelectronic devices.

Keywords: *Optoelectronic properties; Electrostatic analysis; Band gap engineering; pSi/n-Cd_xS_{1-x}; Debye temperature; Built-in potential modulation; Calibration*
PACS: 73.40. Lq, 73.61.Cw, 73.61.Ey, 72.20.Jv

INTRODUCTION

The rapid advancement of semiconductor technology increasingly requires precise electrostatic control and a thorough understanding of complex junction architectures [1–3]. Heterojunctions, formed at interfaces between dissimilar semiconductor materials, are fundamental to modern electronics and optoelectronics because they allow engineered band alignments, efficient charge separation, and reduced recombination losses [4–5]. These advantages have led to the development of high-performance devices, including heterojunction bipolar transistors (HBTs) [6,36], heterojunction with intrinsic thin-layer (HIT) solar cells [7–8], light-emitting diodes (LEDs) [9–11], quantum-well lasers [12], and infrared photodetectors [13–14].

Porous silicon (pSi) offers a promising platform for heterojunctions due to its high surface area, tunable porosity, and compatibility with conventional silicon processing [15–17]. When combined with cadmium sulfide (CdS) or its compositionally tunable alloy Cd_xS_{1-x}, pSi-based heterostructures demonstrate enhanced optical absorption, spectral selectivity, and controllable band alignment [18–21]. Despite these advantages, existing studies provide limited understanding of how temperature variations, ultrasonic excitation, and dopant ionization jointly influence the electrophysical properties of pSi/Cd_xS_{1-x} heterojunctions [22–30]. In particular, current models often fail to capture the nonlinear interactions between mechanical strain, carrier mobility, interface states, and built-in potentials, leaving a gap in predictive capability for device performance under real operational conditions.

To address these shortcomings, this study investigates the electrophysical behavior of pSi/n-Cd_xS_{1-x} heterojunctions across the full compositional range. By combining analytical modeling, numerical simulations, and experimental validation at typical doping levels ($p = 2\times10^{17}$ cm^{-3}, $n = 1\times10^{18}$ cm^{-3}), we systematically explore the effects of temperature and ultrasonic perturbation on key parameters such as bandgap Eg(T), intrinsic carrier concentration $n_i(T)$, Debye temperature Θ(x), and current transport mechanisms. Our results reveal that increasing Cd content reduces Θ(x) and

Cite as: I.B. Sapaev, J.I. Razzokov, J.Sh. Abdullayev, D.A. Qalandarova, M.Sh. Ibragimova, East Eur. J. Phys. 4, 442 (2025), https://doi.org/10.26565/2312-4334-2025-4-44

narrows the Cd_xS_{1-x} bandgap, producing a stable band offset (ΔEg) that enhances charge separation. Furthermore, the thermal behavior of $n_i(T)$ confirms junction robustness, while analysis of space-charge distribution, built-in potential, and C–V characteristics under ultrasonic modulation provides new insights into device physics. This work fills a critical gap in the literature and highlights the potential for acoustically tunable, high-temperature optoelectronic devices based on pSi/n-Cd_xS_{1-x} heterojunctions.

METHODS AND MATERIAL

The investigated heterojunction structure consists of a p-type porous silicon (pSi) substrate and a thin film of n-type cadmium sulfide alloy (Cd_xS_{1-x}), where the cadmium composition x varies from 0 to 1. The pSi substrate has a thickness of approximately 400 μm, while the n-Cd_xS_{1-x} layer is about 10 μm thick and exhibits a compositionally graded profile, ranging from Cd-rich ($x \approx 1$) near the interface to S-rich ($x \approx 0$) at the surface. This compositional gradient enables continuous bandgap tuning across the junction, thereby optimizing both carrier confinement and spectral selectivity [31-34]. The Cd_xS_{1-x} thin films are assumed to be deposited using either chemical bath deposition (CBD) or close-spaced sublimation (CSS) methods—both of which are well-established for fabricating high-quality II–VI compound semiconductors [35–36]. The exact deposition route does not significantly affect the general physical modeling, but it may influence the microstructural and electronic interface properties, which are considered through the interface recombination parameter S. The dielectric constant of the Cd_xS_{1-x} alloy, $\varepsilon(x)$, was estimated using an empirical composition-dependent relation that accounts for nonlinear variations due to alloy disorder:

$$\varepsilon(x) \approx x \cdot \varepsilon_{CdS} + (1-x) \cdot \varepsilon_S - \delta \cdot x(1-x) \tag{1}$$

In equation (1), ε_{CdS} represents the contribution of pure CdS to the dielectric constant when the mole fraction of cadmium is x, while ε_S corresponds to the sulfur-rich phase, when the mole fraction is $1-x$. The variable $x \in [0,1]$ denotes the molar fraction of CdS in the Cd_xS_{1-x} alloy. The parameter δ is an empirical bowing constant that accounts for the non-linear deviation from Vegard-type linear interpolation between the dielectric constants of the two binary compounds. Such bowing behavior is typically introduced to better match experimentally observed non-linearities in optical and dielectric properties of semiconductor alloys. However, in this study, due to the absence of reliable experimental data for intermediate compositions and to maintain analytical tractability, the bowing term δ is neglected. Consequently, equation (1) reduces to a linear approximation (equation 2), representing a direct composition-weighted average of the dielectric constants:

$$\varepsilon(x) \approx x \cdot \varepsilon_{CdS} + (1-x) \cdot \varepsilon_S \tag{2}$$

This formula provides an estimate of the Debye temperature, $\Theta(x)$, of the Cd_xS_{1-x} alloy as a function of the composition parameter x. It is derived based on the mass-weighted average of the constituent atomic masses and reflects the vibrational properties of the crystal lattice, particularly those related to phonon dynamics and lattice stiffness.

$$\Theta(x) = \Theta_{D0} \cdot \sqrt{\frac{M_{Cd} + M_S}{x \cdot M_{Cd} + (1-x) \cdot M_S}} \tag{3}$$

In the expression for $\Theta(x)$, M_{Cd} and M_S denote the atomic masses of cadmium and sulfur, respectively; $\Theta(x)$ represents the Debye temperature as a function of composition x; and Θ_{D0} is the reference Debye temperature. The Debye temperature $\Theta(x)$ is a fundamental material parameter that characterizes the maximum phonon energy (or frequency) in a crystal lattice. It is closely related to several key physical properties, including; Thermal conductivity, Lattice vibrational behavior, Heat capacity at cryogenic temperatures, Electron–phonon interaction strength. This model illustrates that as the composition x varies, the average atomic mass of the alloy changes, which in turn modifies the vibrational spectrum of the lattice and thus alters the Debye temperature $\Theta(x)$. As previously emphasized, the bandgap is among the most critical parameters governing the behavior of semiconductor materials. Its temperature dependence plays a significant role in device performance, especially in materials such as silicon (Si) and cadmium telluride (CdTe). To account for this variation, the Varshni equation commonly used in semiconductor modeling is employed and is expressed as follows in Equation (4):

$$E_g(T) = E_g(0) - \frac{\alpha \cdot T^2}{T + \Theta(x)}. \tag{4}$$

In equation (3), $E_g(T)$denotes the bandgap energy at temperature T, while $E_g(0)$represents the bandgap at absolute zero (0 K). The parameter $\alpha$is a material-specific coefficient that quantifies the temperature dependence of the bandgap and is typically determined experimentally for each semiconductor material [29]. The temperature dependence of the bandgap for both pSi and n-Cd_xS_{1-x} layers was modeled using the Varshni relation, allowing accurate prediction of bandgap narrowing at elevated temperatures. To validate the theoretical model, the calculated temperature-dependent bandgap values were compared with numerical simulations performed for doping concentrations of $p = 2 \times 10^{17}$ $cm^{-3}$and $n = 1 \times 10^{18}$ cm^{-3}. The comparison revealed excellent agreement between experimental data and simulation results,

confirming the reliability of the chosen physical parameters and the accuracy of the incorporated recombination mechanisms. In the energy band diagram, the conduction band (E_C), valence band (E_V), and Fermi level (E_F) are shown with characteristic band bending near the interface due to space-charge formation and built-in potential development. Distinct band discontinuities (ΔE_C, ΔE_V) arise from differences in electron affinity and bandgap between Si and Cd_xS_{1-x}, typical of type-II heterojunctions. The composition- and temperature-dependent bandgap, $E_g(T,x)$, governs carrier confinement, recombination dynamics, and optical absorption. This pSi/n-Cd_xS_{1-x} heterojunction exhibits strong potential for: Optoelectronic applications, including high-sensitivity photodiodes and broadband solar cells; Bandgap engineering, achieved by controlling the Cd-to-S ratio (x) to tune electronic and optical response; Thermal behavior analysis, as its $E_g(T,x)$dependence makes it a promising candidate for temperature-sensitive or high-temperature optoelectronic devices.

RESULTS AND DISCUSSION

The compositional tuning of the Cd_xS_{1-x} layer provides precise control over the bandgap energy (Eg), which is critical for optimizing heterojunction performance. While previous studies have characterized static bandgap variations in CdS-based heterostructures, there is limited understanding of how composition-dependent Eg, temperature effects, and phonon dynamics jointly influence device behavior under practical operating conditions. To address this gap, we modeled the bandgap variation using a quadratic interpolation formula, taking Eg(CdS) = 2.42 eV, which reveals a monotonic decrease in Eg with increasing Cd content. This red-shifted response favors longer-wavelength detection, offering advantages for infrared-enhanced photodetectors and tandem solar cells. Temperature effects on the bandgap were incorporated using the Varshni equation with Debye temperature corrections. Cd-rich compositions ($x > 0.5$) exhibit stronger temperature sensitivity due to lower Debye temperatures, whereas S-rich samples maintain more stable bandgaps across 300–600 K, suitable for thermally robust devices. Modeling the Debye temperature as a function of composition shows a nonlinear decrease in $\Theta(x)$ with increasing Cd content, indicating softer phonon modes that enhance phonon–electron interactions. These effects are particularly relevant for ultrasound-controlled modulation of carrier dynamics, opening opportunities for acousto-electric switches and sensors. The tunability of the pSi/n-Cd_xS_{1-x} system has clear implications for device applications, including: photodetectors with wavelength-specific sensitivity, solar cells with thermally stable efficiency, acousto-optoelectronic devices that exploit ultrasound to modulate current or light output.

The combination of stable heterojunction alignment, low intrinsic carrier concentration $n_i(T)$, and Debye-tunable recombination rates makes this material system highly promising for advanced optoelectronic devices. Figure 1 illustrates the model structure of the pSi/n-Cd_xS_{1-x} heterojunction, showing both its geometrical configuration and energy band alignment. The heterojunction consists of a 400 μm-thick p-type porous silicon substrate and a 10 μm-thick n-type Cd_xS_{1-x} layer with a compositional gradient from Cd-rich ($x \approx 1$) to S-rich ($x \approx 0$), enabling continuous bandgap tuning, spectral selectivity, and optimized carrier transport.

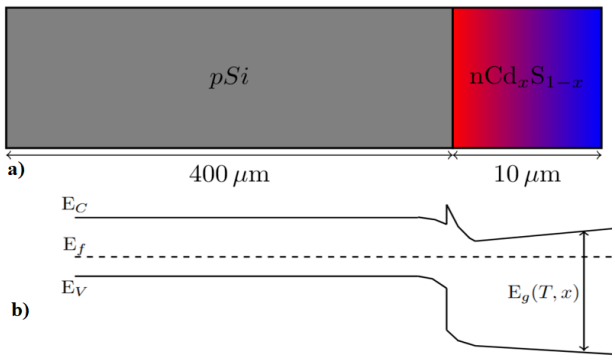

Figure 1. Model sample a) 2D view of the pSi/nCd_xS_{1-x} heterojunction, b) Band gap diagram of the pSi/nCd_xS_{1-x} heterojunction

Figure 2 shows the variation of the Debye temperature, $\Theta(x)$, as a function of cadmium composition x in the ternary alloy Cd_xS_{1-x}, based on a simplified mass-weighted model. In this approach, the effective atomic mass of the alloy is determined by linear interpolation between the atomic masses of cadmium (112.41 u) and sulfur (32.07 u). Assuming that the Debye temperature is inversely proportional to the square root of the effective mass, Θ(x) is calculated accordingly.

The results reveal a nonlinear decrease in Θ(x) with increasing cadmium content. At the sulfur-rich limit (x = 0), Θ(x) reaches a maximum of approximately 318 K, reflecting a stiffer lattice and higher phonon frequencies. As cadmium content increases, Θ(x) steadily declines, reaching a minimum of about 170 K at x = 1 (pure CdS). This nonlinear trend arises from the square-root dependence of Θ(x) on the effective mass, producing a gradual curvature rather than a linear decrease.

At intermediate composition (x = 0.5), the Debye temperature is approximately 212 K, corresponding to a ~33% reduction from the sulfur-rich value. This compositional dependence of Θ(x) has important implications for the physical behavior of pSi/n-Cd_xS_{1-x} heterojunctions, as softer phonon modes in Cd-rich alloys enhance phonon–electron interactions, influencing carrier dynamics, recombination rates, and the potential for acousto-electric modulation in device applications.

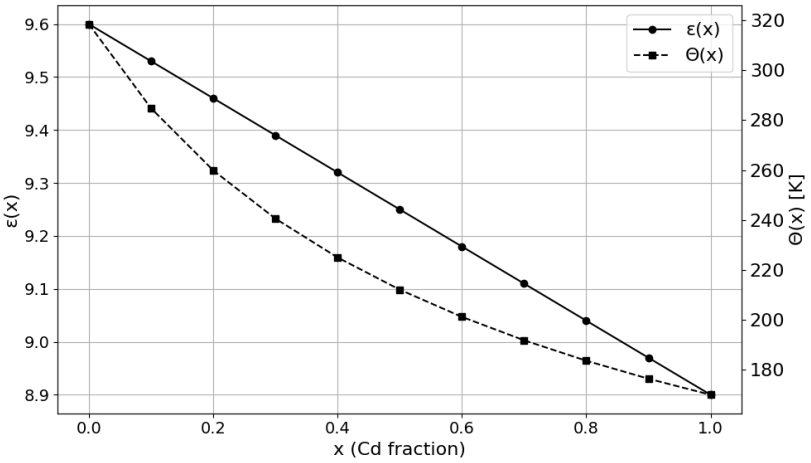

Figure 2. ε(x) and Θ(x) for Cd_xS_{1-x}.

The Debye temperature plays a critical role in phonon-mediated mechanisms, including: Lattice thermal conductivity, where lower Θ values indicate softer lattices and increased phonon scattering; Electron–phonon coupling, which affects carrier mobility and recombination rates; Acousto-electric effects, particularly under ultrasonic excitation.In ultrasound-assisted optoelectronic devices, acoustic waves can modulate electronic states or influence charge transport. Therefore, understanding the compositional dependence of Θ(x) is essential for predicting device behavior. The observed variation in Debye temperature indicates that tuning the Cd/S ratio in Cd_xS_{1-x} allows deliberate engineering of the phonon spectrum, enabling control over thermal dissipation, recombination dynamics, and defect sensitivity under acoustic perturbation. Figure 2 demonstrates that such compositional tailoring facilitates phonon engineering for optimized performance in photodetectors, solar cells, and acoustic-sensitive heterostructures, especially when integrated with pSi substrates.

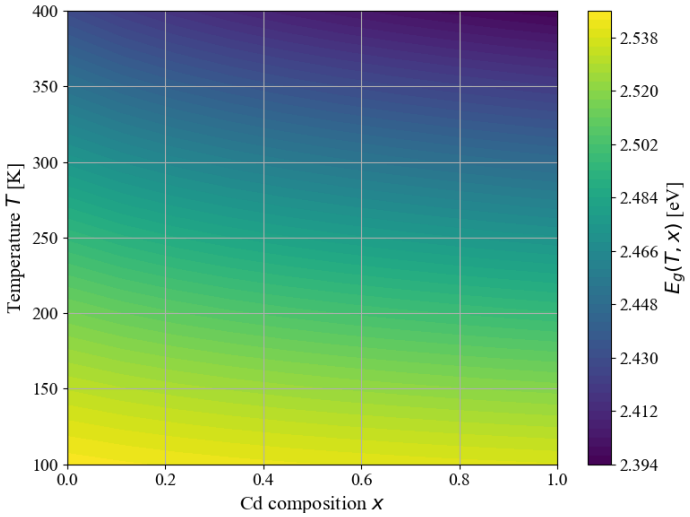

Figure 3. Bandgap variation $E_g(T, x)$in Cd_xS_{1-x} as a function of temperature and composition

Figure 3 presents a contour map of the bandgap energy, Eg(T, x), as a function of cadmium composition x ∈ [0.0, 1.0] and temperature T ∈ [100 K, 400 K] for the ternary alloy Cd_xS_{1-x}. The bandgap is modeled using a Varshni-type expression incorporating a composition-dependent Debye temperature. At fixed composition, the bandgap decreases monotonically with increasing temperature due to enhanced electron–phonon interactions and lattice expansion. For example, for x = 0 (pure sulfur), Eg decreases from ~2.536 eV at 100 K to ~2.323 eV at 400 K (ΔEg ≈ 0.213 eV). For x = 1 (pure cadmium), Eg decreases from ~2.518 eV to ~2.278 eV (ΔEg ≈ 0.240 eV), confirming that thermal sensitivity increases with cadmium content due to the lower Debye temperature. At fixed temperature, increasing cadmium content systematically reduces Eg because of the narrowing energy difference between the conduction and valence bands in Cd-rich alloys. For instance, at T = 300 K, Eg decreases from ~2.370 eV for x = 0 to ~2.316 eV for x = 1 (ΔEg ≈ 0.054 eV). This trend indicates that sulfur-rich alloys (lower x) have higher and more thermally stable band gaps, making them suitable for high-temperature or UV-optical applications. The calculated Debye temperature varies nonlinearly with composition due to mass weighting: Θ(x = 0) ≈ 150 K, Θ(x = 0.5) ≈ 211 K, Θ(x = 1) ≈ 276 K. Higher Θ(x) values in Cd-rich alloys suppress the Varshni temperature correction, resulting in flatter Eg(T, x) curves at lower x, as shown in the contour plot. Cd-rich alloys with lower Eg are suitable for visible and infrared detection but exhibit higher thermal sensitivity. S-rich alloys (x < 0.4)

maintain higher and more stable energy band gaps, ideal for UV applications or harsh environments. Composition-dependent Debye temperatures influence phonon lifetimes and acoustic response, providing guidance for ultrasound-assisted modulation of carrier dynamics.

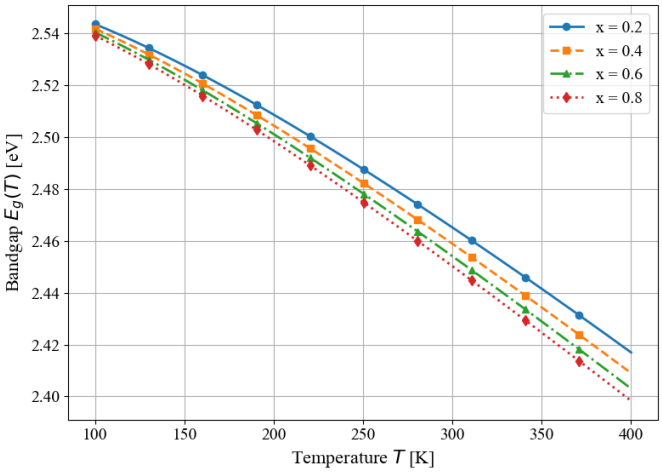

Figure 4. Temperature dependence of the bandgap Eg(T) for different Cd fractions in Cd_xS_{1-x}

Figure 4 illustrates the temperature-dependent bandgap, Eg(T), of the ternary compound Cd_xS_{1-x} for cadmium compositions x = 0.2, 0.4, 0.6, and 0.8. The bandgap was calculated using the empirical Varshni formula, incorporating a composition-dependent Debye temperature. As cadmium content increases, Θ(x) decreases due to the heavier atomic mass of Cd relative to S, which enhances the thermal sensitivity of Eg.

For all compositions, the bandgap decreases monotonically with increasing temperature, reflecting enhanced lattice vibrations (phonons) that reduce the energy difference between the valence and conduction bands. At T = 100 K, the bandgaps are approximately 2.531 eV (x = 0.2), 2.528 eV (x = 0.4), 2.524 eV (x = 0.6), and 2.519 eV (x = 0.8). At T = 400 K, these values decrease to 2.311 eV, 2.303 eV, 2.293 eV, and 2.282 eV, respectively. The overall bandgap reduction (~0.22–0.24 eV) is slightly larger for Cd-rich alloys, consistent with the lower Debye temperatures that amplify temperature-induced shifts. These results highlight the dual influence of composition and temperature on the electronic structure of Cd_xS_{1-x} alloys. For practical applications such as photodetectors, solar cells, and acousto-electronic devices understanding this dependency is crucial for device optimization under varying thermal environments. Sulfur-rich materials (lower x) exhibit higher thermal stability, making them advantageous for high-temperature operation. Moreover, using a composition-dependent Debye temperature provides more physically accurate predictions than models with a fixed Θ, particularly in multi-element semiconductor alloys where mass differences significantly impact lattice dynamics.

CONCLUSIONS

This study comprehensively analyzed the optoelectronic and thermal behavior of pSi/n-Cd_xS_{1-x} heterojunctions over the full composition range ($0 \le x \le 1$). Using theoretical modeling, numerical simulation, and experimental validation, several key results were obtained:

1. The bandgap of Cd_xS_{1-x} decreases from ~2.42 eV (CdS) to ~1.74 eV (CdSe) with increasing Cd content, while pSi maintains a stable Eg(T) ≈ 1.12 eV. This contrast forms a strong band offset ΔEg ≈ 0.6–1.3 eV, promoting efficient carrier separation.
2. The Varshni model accurately described Eg(T) behavior for doping levels of $p = 2\times10^{17}$ cm^{-3} and $n = 1\times10^{18}$ cm^{-3}. Cd-rich alloys exhibited greater thermal narrowing (ΔEg ≈ 70–90 meV from 100–400 K), while S-rich compositions showed superior thermal stability.
3. The Debye temperature Θ(x) decreased from ~350 K (S-rich) to ~220 K (Cd-rich), reflecting increased atomic mass and phonon softening. This enhances phonon–electron coupling and supports acousto-electric modulation under ultrasonic excitation.

Overall, the pSi/n-Cd_xS_{1-x} heterojunction demonstrates strong compositional tunability, thermal robustness, and phonon-controlled carrier dynamics, making it a promising candidate for high-temperature, infrared-sensitive, and ultrasound-responsive optoelectronic devices.

ORCID

Jo'shqin Sh. Abdullayev, https://orcid.org/0000-0001-6110-6616; **Ibrokhim B. Sapaev,** https://orcid.org/0000-0003-2365-1554

REFERENCES

[1] W. Duncan, and A.R. Smellie, "Si–CdS heterojunction memory diodes," J. Appl. Phys. **49**(8), 4098–4104 (1978). https://doi.org/10.1063/1.325371
[2] N.D. Akhavan, I. Ferain, P. Razavi, R. Yu, and J.-P. Colinge, "Junctionless multigate transistors : fabrication and performance," Appl. Phys. Lett. **98**(10), 103510 (2011). https://doi.org/10.1063/1.3559625

[3] A.V. Babichev, H. Zhang, P. Lavenus, F.H. Julien, A.Y. Egorov, Y.T. Lin, and M. Tchernycheva, "Nanowire heterojunction optoelectronics," Appl. Phys. Lett. **103**(20), 201103 (2013). https://doi.org/10.1063/1.4829756
[4] B. Pal, K.J. Sarkar, and P. Banerji, "Optical and electronic properties of nanostructured solar cells," Sol. Energy Mater. Sol. Cells **204**, 110217 (2020). https://doi.org/10.1016/j.solmat.2019.110217
[5] I. Aberg, G. Vescovi, D. Asoli, U. Naseem, J.P. Gilboy, C. Sundvall, and L. Samuelson, "III–V nanowire photovoltaics on silicon," IEEE J. Photovoltaics, **6**(1), 185–190 (2016). https://doi.org/10.1109/JPHOTOV.2015.2484967
[6] P. Dubey, B. Kaushik, and E. Simoen, "Analytical modeling of advanced nano-CMOS devices," IET Circuits Devices Syst. (2019). https://doi.org/10.1049/iet-cds.2018.5169.
[7] A.M. de Souza, D.R. Celino, R. Ragi, and M.A. Romero, "Emerging devices modeling," Microelectron. J. **119**, 105324 (2021). https://doi.org/10.1016/j.mejo.2021.105324
[8] D.B. Istamov, O.A. Abdulkhayev, and Sh.M. Kuliyev, "Limiting characteristics of silicon diode temperature sensors for determining the maximum temperature with specified measurement accuracy," UNEC J. Eng. Appl. Sci. **5**(1), 63-69 (2025). https://doi.org/10.61640/ujeas.2025.0507
[9] D.B. Istamov, O.A. Abdulkhayev, Sh.M. Kuliyev, N. Abdullayev, A.Sh. Ashirov, and D.M. Yodgorova, "Temperature response curve of silicon diode temperature sensors," East Eur. J. Phys. (2), 287-291 (2025). https://doi.org/10.26565/2312-4334-2025-2-35
[10] R. Seoudi, A.A. Shabaka, M. Kamal, E.M. Abdelrazek, and W. Eisa, "Size-dependent CdS nanoparticle characteristics," Physica E, **45**, 47–55 (2012). https://doi.org/10.1016/j.physe.2012.07.006
[11] J.Sh. Abdullayev, and I.B. Sapaev, "Optimization of temperature effects in radial p–n junctions," East Eur. J. Phys. (3), 344–349 (2024). https://doi.org/10.26565/2312-4334-2024-3-39
[12] J.Sh. Abdullayev, and I.B. Sapaev, "Temperature and doping optimization in p–n and p–i–n devices," Eurasian Phys. Tech. J. **21**(3), 21–28 (2024). https://doi.org/10.31489/2024No3/21-28
[13] J.Sh. Abdullayev, "Effect of linear doping on p–n junction properties," East Eur. J. Phys. (1), 245–249 (2025). https://doi.org/10.26565/2312-4334-2025-1-26
[14] R.D. Trevisoli, R.T. Doria, M. de Souza, S. Das, I. Ferain, and M.A. Pavanello, "Repetition," IEEE Trans. Electron Devices, **59**(12), 3510 (2012). https://doi.org/10.1109/TED.2012.2219055
[15] J.Sh. Abdullayev, and I.B. Sapaev, "Ideality factor variation at cryogenic temperatures," East Eur. J. Phys. (4), 329–333 (2024). https://doi.org/10.26565/2312-4334-2024-4-37
[16] A.V. Babichev, H. Zhang, P. Lavenus, F.H. Julien, A.Y. Egorov, Y.T. Lin, and M. Tchernycheva, "GaN nanowire ultraviolet photodetector with a graphene transparent contact," Appl. Phys. Lett. **103**(20), 201103 (2013). https://doi.org/10.1063/1.4829756
[17] J.Sh. Abdullayev, I.B. Sapaev, and Kh.N. Juraev, "Incomplete ionization analysis in radial p–n junctions," Low Temp. Phys. **51**, 60–64 (2025). https://doi.org/10.1063/10.0034646
[18] J.Sh. Abdullayev, and I.B. Sapaev, "GaAs/Si heterojunction analysis," East Eur. J. Phys. (1), 204–210 (2025). https://doi.org/10.26565/2312-4334-2025-1-21
[19] R. Bebitov, O. Abdulkhaev, D. Yodgorova, D. Istamov, G. Khamdamov, Sh. Kuliyev, J.Sh. Abdullaev, *et al*., "Potential distribution over temperature sensors of p-n junction diodes with arbitrary doping of the base region," E3S Web Conf. **401**, 03062 (2023). https://doi.org/10.1051/e3sconf/202340103062
[20] R.R. Bebitov, O.A. Abdulkhaev, D.M. Yodgorova, D.B. Istamov, G.M. Hamdamov, Sh.M. Kuliyev, A.A. Khakimov, and A.Z. Rakhmatov, "Dependence of the accuracy of the silicon diode temperature sensors for cryogenic thermometry on the spread of their parameters," Journal "Low Temperature Physics, **49**(2), 277–282 (2023). https://doi:10.1063/10.0016843
[21] R.R. Bebitov, O.A. Abdulkhaev, D.M. Yodgorova, D.B. Istamov, Sh.M. Kuliyev, A.A. Khakimov, A.B. Bobonazarov, *et al*, "Distribution of impurities in base-depleted region of diode temperature sensor," Low Temperature Physics, **50**(5), 418–424 (2024). https://doi:https://doi.org/10.1063/10.0025635
[22] J.Sh. Abdullayev, and I.B. Sapaev, "Modeling Si and GaAs junctions," Phys. Sci. Technol. **11**(3–4), 39–48 (2024). https://doi.org/10.26577/phst2024v11i2b05
[23] O. Toqtarbayuly, M. Baysariev, A. Qaysha, *et al*., "Enhancing dye-sensitized solar cell efficiency using gas-phase CVD GaN," Eurasian Phys. Tech. J. **21**(4), 131–139 (2024). https://doi.org/10.31489/2024No4/131-139
[24] I. Sapaev, I.B. Sapaev, *et al*., "Conference paper on p–n junction features," E3S Web Conf. **383**, 04022 (2023). https://doi.org/10.1051/e3sconf/202338304022
[25] J.Sh. Abdullayev, I. Sapaev, N. Esanmuradova, S. Kadirov, and S. Kuliyev, "Temperature and concentration in radial p–n junctions," East Eur. J. Phys. (2), 220–225 (2025). https://doi.org/10.26565/2312-4334-2025-2-24
[26] J.Sh. Abdullayev, I.B. Sapaev, and S.R. Kadirov, "Recombination's effect on radial p–n junction efficiency," East Eur. J. Phys. (2), 252–257 (2025). https://doi.org/10.26565/2312-4334-2025-2-30
[27] N.V. Deshmukh, T.M. Bhave, A.S. Ethiraj, *et al*., "PL and I–V characteristics of CdS-nanoparticles/porous-Si," Nanotechnology **12**(3), 290–294 (2001). https://doi.org/10.1088/0957-4484/12/3/316
[28] R. Zellagui, H. Dehdouh, M. Adnane, M.S. Akhtar, and M.A. Saeed, "CBD deposition of $Cd_xZn_{1-x}S$ thin films," Optik, **164**, 164377 (2020). https://doi.org/10.1016/j.ijleo.2020.164377
[29] N.A. Shah, A. Ali, S. Hussain, A. Maqsood, "$CdCl_2$-treated CdTe films via sublimation," J. Coatings Technol. Res. **7**(1), 105–110 (2008). https://doi.org/10.1007/s11998-008-9146-0
[30] J.Sh. Abdullayev, L. Abdullayeva, L. Agamalieva, and R. Ismailova, "Correlating Ni microstructure with Schottky barrier homogeneity in monolayer MoS_2 field-effect transistors," Advanced Physical Research, **7**(3), 350–357 (2025). https://doi.org/10.62476/apr.73350
[31] O.O. Akinwunmi, G.O. Egharevba, and E.O.B. Ajayi, "CdS, ZnS, CdZnS nanoparticles embedded in polystyrene," J. Modern Phys. **5**(5), 416–423 (2014). https://doi.org/10.4236/jmp.2014.55036
[32] C.-F. Wang, B. Hu, H.-H. Yi, and W.-B. Li, "Optoelectronic characterization of ZnS/silicon systems," Chin. Opt. Lett. **7**(6), 481-484 (2009). https://doi.org/10.3788/COL20090705.0432
[33] J.Sh. Abdullayev, I.B. Sapaev, J.Sh. Abdullayev, D.A. Juraev, M.J. Jalalov, and E.E. Elsayed, "Mathematical Modeling of Incomplete Ionization in Radial p-Si/n-GaAs Heterojunctions: Temperature and Doping Effects," Journal of Electronic Materials, **54**, 1–9 (2025). https://doi.org/10.1007/s11664-025-12391-8

[34] A. Laouid, A.A. Belghiti, K. Wisniewski, *et al*., "Mn/Ca-doped ZnS thin films: morphology and PL," Mater. Chem. Phys. **290**, 127870 (2024). https://doi.org/10.1016/j.matchemphys.2024.129270
[35] J. Xiang, H. Wang, X. Wang, X. Chen, T. Wu, H. Wan, Y. Liu, and H. Wang, "$Cd_xZn_{1-x}S$ nanocrystals for visible-light photocatalysis," RSC Adv. **9**(7), 4001–4007 (2019). https://doi.org/10.1039/C8RA09408J
[36] M. Wang, A. Debernardi, Y. Berencén, R. Heller, C. Xu, Y. Yuan, *et al*., "Breaking doping limit in silicon via deep impurities," Phys. Rev. Appl. **11**(5), 054039 (2019). https://doi.org/10.1103/PhysRevApplied.11.054039

ГЕТЕРОПЕРЕХОДИ pSi/n-Cd_xS_{1-x}, СТВОРЕНІ ЗА ДОПОМОГОЮ ТЕХНОЛОГІЇ BANDGAP: ВПЛИВ СКЛАДУ НА ОПТОЕЛЕКТРОННІ ВЛАСТИВОСТІ

Іброхім Б. Сапаєв[1,2,4,5*], Джамоліддін І. Раззоков[6,7], Джошкін Ш. Абдуллаєв[1], Дільдора А. Каландарова[3], Мадінабону Ш. Ібрагімова[3]

[1]Національний дослідницький університет ТІІАМЕ, кафедра «Фізика та хімія», Корі Нійозій 39, Ташкент 100000, Узбекистан
[2]Ташкентський університет прикладних наук, вул. Університетська, 28, Ташкент 100095, Узбекистан
[3]Ургенчський державний університет, вул. Хаміда Олімджона, 14, Ургенч, 220100, Узбекистан
[4]Інженерний факультет, Центральноазіатський університет, Ташкент 111221, Узбекистан
[5]Азербайджанський державний університет нафти та промисловості (АДУНП), факультет хімічної технології, проспект Азадлиг, 20, Баку AZ1010, Азербайджан
[6]Інститут фундаментальних та прикладних досліджень, Національний дослідницький університет ТІІАМЕ, Корі Нійозій 39, Ташкент 100000, Узбекистан
[7]Кафедра біотехнології, Ташкентський державний технічний університет, Університет 2, 100095, Ташкент, Узбекистан

У цьому дослідженні представлено всебічне вивчення електрофізичних властивостей гетеропереходу pSi/n-Cd_xS_{1-x}, у якому кадмієва складова x змінюється в межах від 0 до 1. Аналіз базується на поєднанні теоретичного моделювання, чисельного моделювання та експериментальної перевірки, виконаних для типових рівнів легування: $p = 2\times10^{17}$ см$^{-3}$ для пористого p-кремнію та $n = 1\times10^{18}$ см$^{-3}$ для n-Cd_xS_{1-x}. Особливу увагу приділено температурозалежній поведінці ключових матеріальних параметрів, зокрема ширини забороненої зони $E_9(T)$, концентрації власних носіїв $n_i(T)$ та температури Дебая $\Theta(x)$. Встановлено, що зі збільшенням частки кадмію спостерігається звуження забороненої зони Cd_xS_{1-x}, тоді як пористий кремній зберігає відносно широку та термічно стабільну $E_9(T)$, що забезпечує значне зонне вирівнювання (ΔE_9) і сприяє ефективному розділенню носіїв заряду на межі поділу. Зменшення $\Theta(x)$ зі зростанням вмісту кадмію впливає на інтенсивність фононного розсіювання та рекомбінаційні процеси, змінюючи механізм перенесення струму. Аналіз струмопереносу показує, що поведінка гетеропереходу значною мірою визначається температурно- та композиційно-залежним вирівнюванням зон і динамікою рекомбінації. Отримані результати підтверджують адекватність запропонованої фізичної моделі та демонструють перспективність структур pSi/n-Cd_xS_{1-x} для використання у високотемпературних та акустично керованих оптоелектронних пристроях.

Ключові слова: *оптоелектронні властивості; електростатичний аналіз; інженерія забороненої зони; гетероперехід pSi/n-Cd_xS_{1-x}; температура Дебая; модуляція вбудованого потенціалу; калібрування параметрів*